Current Characteristics of Defective GNR Nanoelectronic Devices

Konstantinos Rallis
Universitat Politècnica de Catalunya
Barcelona, Spain

Panagiotis Dimitrakis
NCSR Demokritos
Athens, Greece

Ioannis Karafyllidis
Democritus University of Thrace
Xanthi, Greece

Antonio Rubio
Universitat Politècnica de Catalunya
Barcelona, Spain

Georgios Ch. Sirakoulis
Democritus University of Thrace
Xanthi, Greece

ABSTRACT

The most promising Graphene structures for the development of nanoelectronics and sensor applications are Graphene nanoribbons (GNRs). GNRs with perfect lattices have been extensively investigated in the research literature; however, fabricated GNRs may still suffering from lattice flaws, the possible effect of which, on the operation of the circuitry comprised by GNR based devices, has not attracted significant interest. In this paper, we investigate the effect of lattice defects on the operational behavior of GNRs using the Non-Equilibrium Green's function (NEGF) method combined with tight-binding Hamiltonians targeting to the resulting nanoelectronic devices and circuits functionalities. We focus on butterfly-shaped GNRs, which have been proven to successfully function as switches that can be used as building blocks for simple Boolean gates and logic circuits. Analyses of the most common defects, namely the single and double vacancies, have been adequately performed. The effect of these vacancies was investigated by inserting them in various places and concentrations on the corresponding GNR based nano-devices. The computation results indicate the effect on lattice defects on the important operational device parameters including the leakage current, I_{ON}/I_{OFF} and, finally, current density, which will determine the viability of GNR computing circuits.

CCS CONCEPTS

• **Hardware → Defect-based test**; **Carbon based electronics**.

KEYWORDS

Graphene, Graphene nanoribbon (GNR), defects, Nanoelectronics

ACM Reference Format:
Konstantinos Rallis, Panagiotis Dimitrakis, Ioannis Karafyllidis, Antonio Rubio, and Georgios Ch. Sirakoulis. 2022. Current Characteristics of Defective GNR Nanoelectronic Devices. In *17th IEEE/ACM International Symposium on Nanoscale Architectures (NANOARCH '22), December 7–9, 2022, Virtual, OR, USA.* ACM, New York, NY, USA, Article 111, 6 pages. https://doi.org/10.1145/3565478.3572538

Permission to make digital or hard copies of all or part of this work for personal or classroom use is granted without fee provided that copies are not made or distributed for profit or commercial advantage and that copies bear this notice and the full citation on the first page. Copyrights for components of this work owned by others than ACM must be honored. Abstracting with credit is permitted. To copy otherwise, or republish, to post on servers or to redistribute to lists, requires prior specific permission and/or a fee. Request permissions from permissions@acm.org.
NANOARCH '22, December 7–9, 2022, Virtual, OR, USA
© 2022 Association for Computing Machinery.
ACM ISBN 978-1-4503-9938-8/22/12…$15.00
https://doi.org/10.1145/3565478.3572538

1 INTRODUCTION

Since its first successful isolation in 2004, Graphene has attracted lots of attention from the research community [Novoselov et al. 2004, 2007]. Among its many forms, Graphene nanoribbons are one of the most promising for further employment in nanoelectronic devices for computing [Cotofana et al. 2018], due to their exceptional properties such as their high electron mobility, their thermal conductivity and overall their ability to withstand high current densities [Jang et al. 2016]. However, the very significant aspect for Graphene to retain the aforementioned properties is its shape. Carbon atoms in GNRs form hexagonal unit cells connected together resulting to an one-atom thick lattice. In the ideal case, the grid is pristine with no presence of defects, vacancies, adsorbed atoms or any other form of anomaly. Most of the time, though, this case is not true [Banhart et al. 2011]. The forming process of Single Layer Graphene (SLG) nanodevices includes mainly the growth of Graphene at large areas on Cu-foils with the application of the CVD method and the transfer of grown Graphene sheets on the desired substrates. Both of the aforementioned steps are susceptible to inducing defects on the GNR grid. Those defects are mainly attributed to the growth rate [Chin et al. 2018], the quality of the Cu foils [Zhang et al. 2016] as well as the transfer process of Graphene to the desired substrates [Liu et al. 2015].

Graphene devices based on SLG have been extensively used for the realization of switches that comprise nanoelectronic circuits. The conductance of such devices can be tuned by different means and has been accomplished by exploiting the topology awareness of Graphene [Jiang et al. 2018; Karafyllidis 2014], by using electric bias or magnetic fields [Moysidis et al. 2020]. With such ways, GNR based devices have been applied to the realisation of nanocomputational circuits that operate similar to CMOS like architectures but with optimal characteristics and, at the same time, they are also CMOS compatible [Jiang et al. 2019]. Apart from that they have been used for other beyond CMOS circuitry, like multi valued logic circuits [Rallis et al. 2018], and neurons [Wang et al. 2020]. Thus, GNR based devices seem to be able to cover the whole spectrum of nanocomputing circuits, spanning also from classic Neumann to beyond von Neumann computing architectures. All this flexibility makes such devices a very promising candidate to pave the way at the post CMOS era.

On the other hand, recent research on Graphene, in both theoretical and experimental level, have indicated the strong connection between the shape of the Graphene grid with its properties, and, more specifically, its electric properties, which has been also used as a conductance tuning technique. The pristinity and the symmetry of the grid plays a significant role to the device behavior, and this

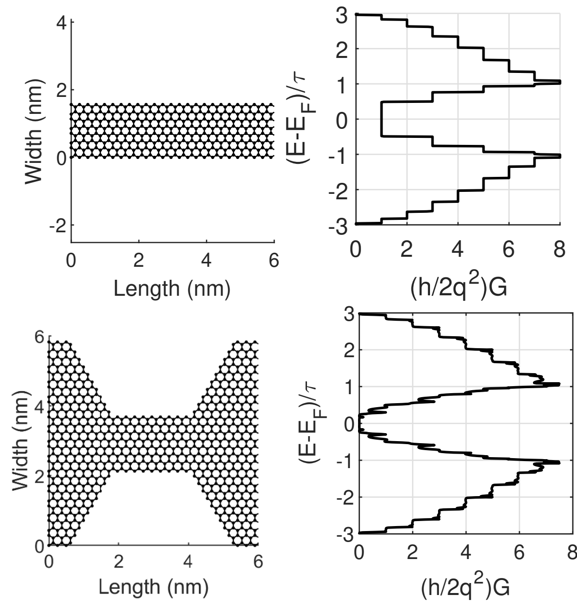

Figure 1: *Top row*: The grid of a pristine zig zag Graphene nanoribbon (zGNR) and its conductance dispersion diagram shown on the right side of the top row. The absence of band gap is obvious. *Bottom row*: A butterfly shaped GQPC device, a small band gap appears around the Fermi energy level (zero in the y-axis) induced by the geometry.

raises the question of the effect that the aforementioned induced defects can possibly have. The conductance of a single GNR device has been found to be vulnerable to lattice defects of different kinds [Rallis et al. 2021]. Thus, it is obvious that defects will have an impact on the ability of GNR devices to operate as switches and synthesize operational and of optimal performance circuits. The viability of GNR devices necessitates the investigation on how severe the always-present fabrication defects affect their operation, and to what extent they can be present, without deteriorating the resulting circuit operation.

In this paper, we aim to further explore the effect of the single and double vacancy defects on the electric properties of GNRs. We try to investigate how the resulting inaccuracy of the fabrication process may affect the computing capabilities and the properties of GNR based devices. Thus we calculate with the application of Tight Binding Hamiltonians (TBH) and the Non-Equilibrium Green's Function method (NEGF), the leakage current of defective devices with different defect concentrations as well as the current I_{ON}/I_{OFF} ratio, as representative metrics for the switching capabilities of a device. The results found confirm the expected effect of defects on the conductivity of the under investigation GNR devices and the resulting circuit operation and in conjunction with the leakage current measurements. Overall, the simulation results on lattice defects are in agreement with theoretical and experimental studies by indicating the major significance of edge states and grid symmetry in GNR´s electronic behavior. In conjunction with the crucial leakage current measurements, the effect of defects is extended to the field of Graphene circuits and their switching operation.

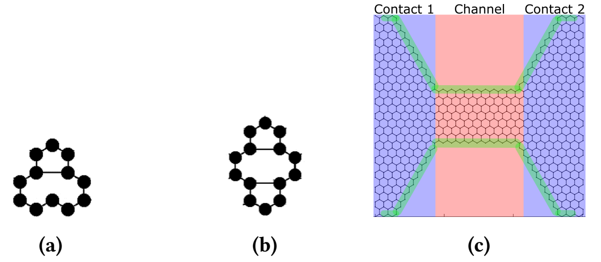

Figure 2: (a) A single vacancy with two available carbon atoms bonded $V1$(5-9) in Graphene lattice, (b) Graphene lattice with a double vacancy $V2$(5-8-5) and (c) GQPC grid's with marked regions. Blue color marks the contacts region, red color marks the channel region and green color marks the edges.

2 GRAPHENE NANORIBBONS

Graphene can be constructed and used in various different forms like Graphene Nanotubes, Graphene flakes and dots, Bi-Layer or Multilayer Graphene, and GNRs, with most of them being able to be utilized in nanoelectronic applications. In particular, GNRs are very narrow sheets of SLG, having a width smaller than $100nm$. They can be characterized by the shape of their edges as zig-zag GNRs (zGNRs) and armchair GNRs (aGNRs). In Figure 1, a zGNR is depicted at the first row in the left, as well as its dispersion diagram on the right. The dispersion diagram practically shows the conductance for different energy levels around Energy Fermi, where the zero point on Y-Axis indicates the Energy Fermi. From this diagram occurs that, for a pristine zGNR, there is no energy gap, and there is no energy level with conductance equal to zero. This also reveals one of the most significant obstacles for the incorporation of Graphene in electronic devices: Graphene is a zero bandgap material. Notwithstanding, there have been many different approaches by the research community that tackle this problem, like the previously mentioned application of electrostatic or magnetic means, and also the specific stacking [Aoki and Amawashi 2007] and twisting of Graphene layers [Yankowitz et al. 2019] and the exploitation of Graphene's topology awareness. For our investigation, we leverage the ability of Graphene to change its electric properties with the change of its dimensions and we use Graphene Quantum Point Contacts (GQPCs). A GQPC is the butterfly shaped device, which is visible in Figure 1 at the second row of Figure in the left. This device is based on the well-known idea of quantum point contacts and has been proven to be an efficient switch, suitable for electronic circuits too [Karafyllidis 2014]. The energy dispersion diagram of this device indicates that this time, around Fermi level, the conductance is zero.

3 MODELLING AND COMPUTATION METHOD

For the proposed simulations, the GQPC devices under test are based on SLG. Even though SLG QPCs are more difficult to be fabricated and Bi-Layer QPCs are more commonly reported in bibliography, the earlier provide more discrete and easy to investigate structures (and mainly edge states), delivering results that can be easily expanded later to Bi-Layer devices. They have a total length

of $6.026nm$ ($30\sqrt{2} \times \alpha$), where α is equal to $0.142nm$. The width of the shortest region in the middle is equal to $1.562nm$ (11α), while the maximum width of the larger region is equal to $5.822nm$. There is a linear reduction from the maximum width of the larger area to the short area in the middle, through which the atoms retain their pristine zig-zag pattern. Thus the device can be separated to two different regions of interest, the short region in the middle which is called the channel and is marked in Figure 2(c) with red color, and the two wider, trapezoidal regions, which are called the contacts and are marked in Figure 2(c) with blue color. Those regions will be examined separately.

For the calculation of the provided results of the ON/OFF ratio, the current density and the leakage current, the Non Equilibrium Green's Function Method (NEGF) [Datta 2000, 2012] is used, along with the Tight-Binding Hamiltonians (TBH) [Bena and Montambaux 2009; Reich et al. 2002]. The NEGF method, is a very powerful tool, appropriate for simulating devices that are regulated by quantum transport phenomena, such as the ballistic transport effect of GNR devices. The TBH is leveraged in order to describe the interconnections between neighbouring atoms and thus encapsulate the defects in our simulations. TBH is given by:

$$H = -\tau_0 \sum_{i,j} \hat{c}_i \hat{c}_j^\dagger, \tag{1}$$

where $\hat{c}_i$, $\hat{c}_j^\dagger$ are the annihilation and creation operators, while τ_0 is the factor that describes the connection strength between nearest neighbour atoms and has been computed to be equal to approximately $-3eV$ [Chico et al. 1996]. Through TBH, we are able to introduce to the proposed modelling approach, the desirable device geometry, or any other lattice anomaly. This geometry is used then by the NEGF method for the conductance calculations, which are then handled for the production of other needed metrics such as current, current density, resistance and thus ON/OFF ratio. This method can be briefly described by the following four (4) equations:

$$G^R = [EI - H - \Sigma_L - \Sigma_R]^{-1}, \tag{2}$$

$$G^n = G^R \Sigma^{in} G^A, \tag{3}$$

$$A = i(G^R - G^A). \tag{4}$$

$$G(E) = \frac{2q^2}{h} Trace[\Gamma_L G^R \Gamma_R G^A]. \tag{5}$$

The NEGF method has been extensively analyzed in bibliography [Datta 2000]. Compactly, equation (2) calculates the retarded Green's function, taking under consideration the TBH, as well as the number of contacts of the investigated device. In correspondence, equation (3) calculates the electron density at a specific energy level, while equation (4), similarly, resembles the density of available states (DoS). Finally, with equation (5) the proposed method uses the results produced already in order to compute the conductance of a GNR device for different energy levels. The conductance can be then applied into the Landauer Formula in order to calculate the current flowing through the device, depending on the applied potentials, and any other relative values [Datta 2005]. The integral expression of the Landauer formula for current calculation is:

$$I = \frac{q}{h} \int_{-\infty}^{\infty} (f_L(E) - f_R(E)) \frac{G(E)}{q^2/h} \, dE \tag{6}$$

where, q is the electron charge, h the Planck constant, $f_L(E)$ and $f_R(E)$ are the Fermi energies for the left and right contact, respectively, and $G(E)$ is the conductance of the device, calculated by NEGF.

4 DEFECTS IN GNRS

This investigation mainly focuses on the simplest forms of Graphene lattice defects, which are also interconnected with one another, namely the single and the double vacancy. Practically, the double vacancy is produced when two neighbouring single vacancies occur. Figure 2(a) shows the Graphene with a single vacancy, which is referred in the bibliography as $V1(5-9)$, due to the two different shaped structures that consist of 5 and 9 atoms. There is also the double vacancy (shown in Figure 2(b)), which is also referred in bibliography as $V2(5-9-5)$ for the same reason, i.e. because of the three different constructs with 5, 9 and 5 atoms each one respectively, from top to bottom [Banhart et al. 2011]. The latter is also reported to be the most thermodynamically stable one, having a migration energy of $7eV$, that makes it almost stationary [Li et al. 2017]. This stability is mainly attributed to the fact that in the case of $V2$, there is no free electron available for making it chemically reactive with its environment, while in the case of $V1$, chemical reactivity is present. There are also other kinds of structural lattice defects like the Stone-Wales defects, the attachment of adatoms, the atoms substitutions, as well as line defects such as the atom dislocations and the grain boundaries defects [Tian et al. 2017], which are not examined in this context.

As it appears from the aforementioned Figures, after the removal of atoms, either one or two, a new bond is considered to be created between the atoms that are now available. For the case of $V1$, there are three atoms available for bonding, which shape an equilateral triangle, meaning that they have the same distance from each other. Thus, the two that will be connected together with a new bond are chosen randomly. The case is not the same with the $V2$ vacancy. This time, there are four different atoms that are available for bonding. However, the bonds are formed only between the atoms with the shortest distance. Bonding between diagonal atoms is not thermodynamically stable.

The reported new bonds have to be modelled and included in the simulation, and this becomes possible through the TBH. Those new bonds do not have the same length with the bonds of a pristine Graphene grid. This length that was previously equal to the lattice constant $\alpha = 0.142nm$, now becomes equal to $r = \sqrt{(3)} \times \alpha\ nm$. This parameter can be included through the aforementioned overlap integral (τ). In its generalized form the new overlap integral for any bond of length r, can be calculated as:

$$\tau_{BOND} = \tau_0 \times \alpha / r^2 \tag{7}$$

For the following simulations, the number of defects tested is varying from as low as five (5) defects up to one hundred (100) defects, unless differently reported. Considering that the total number of atoms in the investigated structure is eight hundred eighty four (840), this means that our simulations span from 0.6% up to 12% percentage of defects. Initiating from five (5) defects, our simulations are performed in an additive manner, meaning that five (5) more vacancies are randomly added each time to the previous formation. For every specific number of defects, ten (10) different simulations

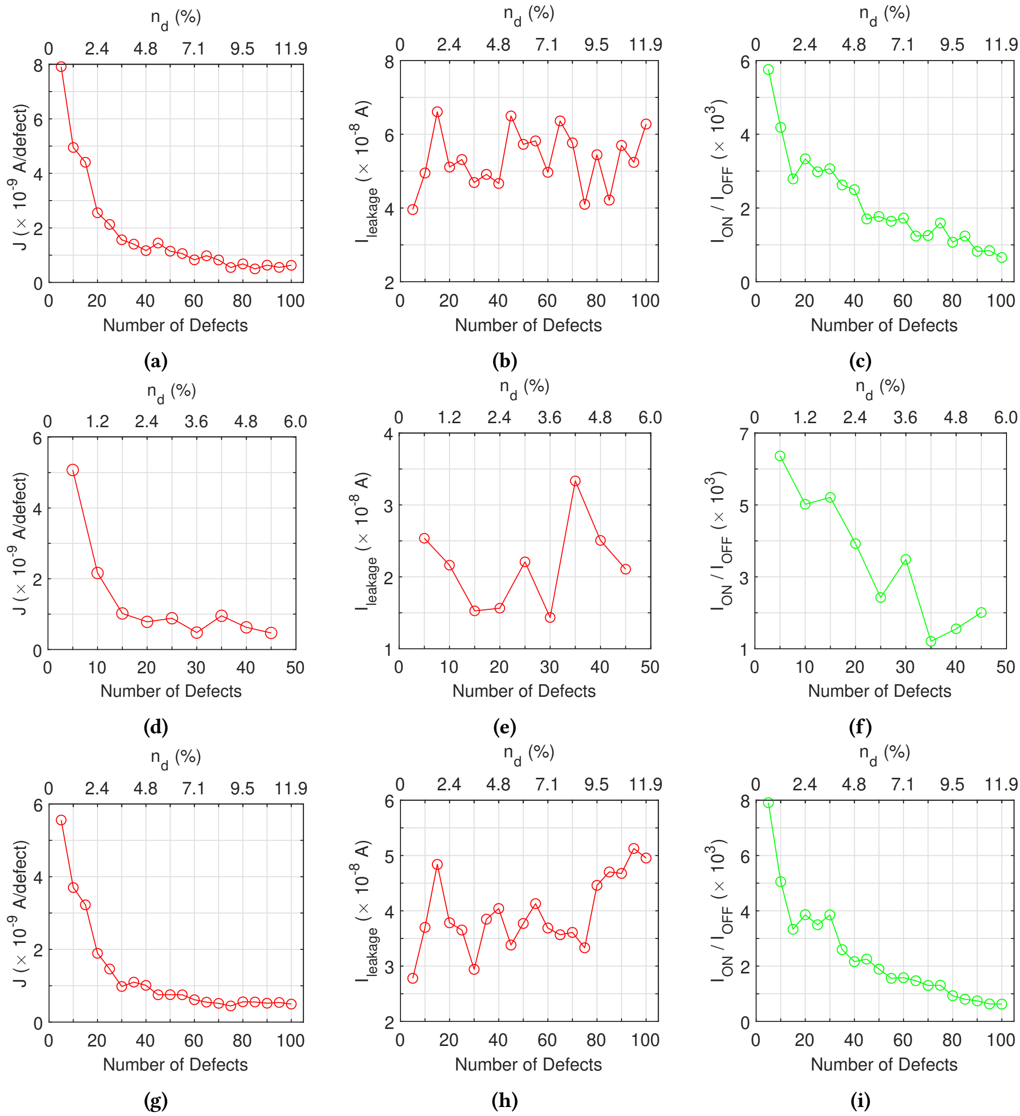

Figure 3: (a), (d), (g) Current density diagrams at $10mV$ (leakage current) calculated for different defect concentrations in the bulk of contacts, channel and both channel and contact, respectively. (b), (e) (h) The change of leakage current (at $10mV$) on the number of lattice defects in the bulk of contacts, channel and both channel and contacts, respectively. (c), (f), (i) I_{ON}/I_{OFF} ratio to the number of defects in the bulk of contacts, channel and both channel and contacts regions, respectively.

are executed, with different vacancy locations, and the final results are produced as the mean value of those ten (10) repetitions.

For every separate simulation case, three (3) different metrics are examined, and thus three (3) corresponding but different graphs are produced. The first is the current density to the number of defects. The current density that is calculated here practically is the current flowing through the device at $10mV$, divided by the number of defects, thus, its unit of measurement is A / N_o of defects (J). The second is the leakage current; more specifically, as we are examining a simple volatile current switch, and due to the absence of a threshold similar to that in silicon transistors, we are considering the current at a very low voltage, namely $10mV$, as the leakage current of this device. And finally, another significant parameter taken under consideration, decisive for the successful operation of a switch, is the I_{ON}/I_{OFF} ratio. The I_{OFF} is considered to be the current at $10mV$, the aforementioned leakage current, and the I_{ON} the current flowing at $0.5V$. This value is selected based on the operating voltage of GNR gates on [Moysidis et al. 2018].

5 BULK DEFECTS AT GNRS

We proceeded with the simulations of defects that were induced only in the bulk area of a GNR. In particular, by the term bulk we refer to all those atoms of the GNR that do not belong to the edge, i.e. to the outer (top or bottom) row of the GNR's atoms, or as clearly previewed in Figure 2(c), the green color marked area.

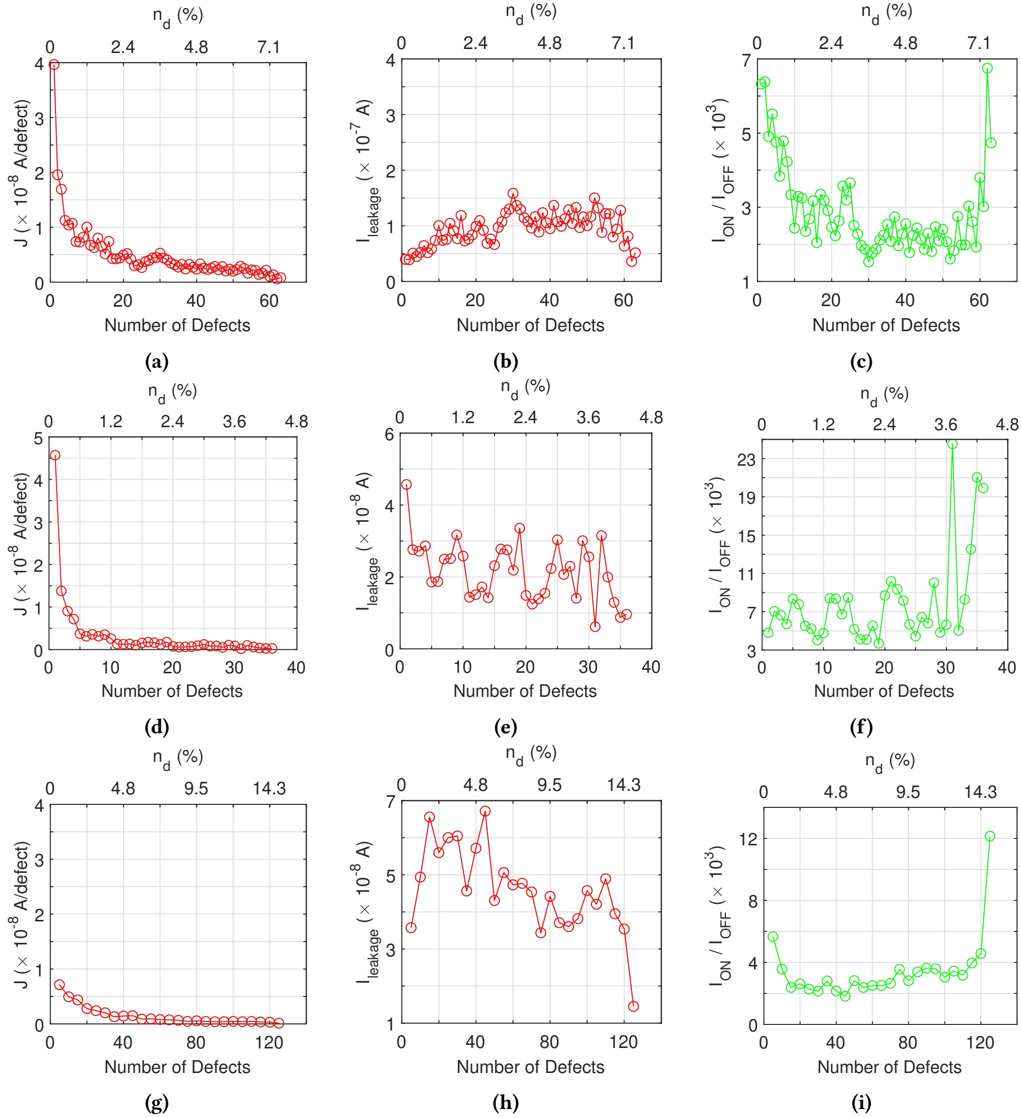

Figure 4: (a), (d), (g) Current density diagrams at $10mV$ (leakage current) calculated for different defect concentrations in the edges of contacts, channel and both channel and contact, respectively. (b), (e) (h) The change of leakage current (at $10mV$) on the number of lattice defects in the edges of contacts, channel and both channel and contacts, respectively. (c), (f), (i) I_{ON}/I_{OFF} ratio to the number of defects in the edges of contacts, channel and both channel and contacts regions respectively.

Following the area device separation that we thoroughly presented in Section 4, we first apply defects of different densities in the two trapezoidal regions, namely the contacts (see Figure 2(c)). What we observe is presented in Figures 3(a), 3(b), and 3(c), respectively. The leakage current in Figure 3(b) seems to be randomly affected by the defects and to not follow a specific tendency. Notwithstanding, due to the fact that the leakage current seems to have a mean value of around $5 \times 10^{-8}A$, the current density in Figure 3(a) seems to be minimized after almost thirty five (35) defects to just $1\times10^{-9}A/defect$. This is a clear statement that leakage current remains practically intact to the increase of defects for up to $n_d = 12\%$ concentration. The I_{ON}/I_{OFF} ratio, has a linear tendency, and decreases from 6, 000 to 1, 000. Considering that the leakage current has a steady mean value, this means that the maximum conductance of the device is almost linearly decreasing with the increase of defects, especially after the first fifteen (15) vacancies $n_d = 1.2\%$.

After the examination of the contacts region, we move on with the introduction of increased defect densities at the bulk of the channel area of a butterfly shaped GNR device (as seen in Figure 2(c)). In this area, there are also some similarities with the previous one. Figure 3(d) shows an abrupt decrease of the current density, which caps to the lowest value of 1×10^{-9} A for only fifteen (15) defects (around $n_d = 1.8\%$). This is almost identical to the previously reported behavior, indicating, however, that the channel drastically affects the operation of the device. The leakage current is again

variable and seems to have a median value of around $2.2 \times 10^{-8} A$. Like the contacts' case, this time again the ON/OFF ratio of the device linearly decreases with the increase of defects, implying a linear decrease of the maximum conductance of the device.

The last case of examining the defects in the bulk of a GNR device, involves the simultaneous appearance of defect concentrations both at the contacts and at the channel. This case as shown in the graphs seems to be a superposition of the previous two. At around twenty five (25) to thirty (30) defects, the current density reaches a minimum value, while the leakage current seems to have a mean value of 3.7. Again the ON/OFF ratio decreases linearly, in a very similar manner to that of the first case shown in Figure 3(c).

6 EDGE DEFECTS AT GNRS

In this Section, the simulations of defects are concentrated on the edges of the GNR devices. Only the outer rows on the top side and the bottom side are affected by vacancies, while the bulk of the device remains intact. Referring to Figure 2(c), the edges are marked with green color. In the same manner with our previous simulations, we are first examining the effect of edge defects at the contacts region. This time, the behavior of the device is more interesting. The leakage current which is presented in Figure 4(b) slightly increases, with a small ratio until a vacancy concentration of $n_d = 3.6\%$. After that threshold, it remains practically steady, and as the defect density increases up to $n_d = 7\%$, it starts to reduce, until reaching its initial value. This is also reflected on the current density graph of Figure 4(a). The ON/OFF ratio of Figure 4(c) also develops a local minimum at a $n_d = 3.6\%$ defective grid and after hitting a plateau, abruptly increases to almost initial values.

Similar behavior also is depicted in the second row of Figure 4, which corresponds to devices with defective edges of their channel. In this case, however, the mean value of leakage current remains almost constant, and reaches levels of almost an order of magnitude lower than in the case of edge defective contacts. The ON/OFF ratio also increases slowly and abruptly spikes up to an order of magnitude higher value, at a defect density of $n_d = 4.2\%$.

Finally, the last case refers to defects distributed in the edges of both contacts and channel with rather similar behavior. The analysis of defective edge behavior verifies the significance of edge states and symmetry to the behavior of GNRs. This peculiar performance boost after a specific value of defect concentration is attributed to the fact that the outer rows are severely damaged, and the rows just-below them begin to act as the new edges. Thus, we are gradually led to the behavior of a pristine GQPC device with narrower width.

7 CONCLUSIONS

In this work, we have simulated the effect of the lattice defects on the current switches utilizing butterfly-shaped GNRs. Comprehensive simulations revealed that the leakage current and the ON/OFF current ratio are modulated by defect concentration. More specifically, the edge defects contribute significantly to the leakage current increase by nearly an order of magnitude. On the contrary, the channel defects do not cause a remarkable increase in leakage current. Also, we have introduced as a figure-of-merit, the current per defect. Further work is necessary to investigate the physical mechanisms causing the current modulation by GNR lattice defects and their representation on TBH.

ACKNOWLEDGMENTS

This research was supported in part by the Spanish MCIN/AEI/ 10.13039/501100011033, Project PID2019-103869RB-C33 and grant 391 (with the support of the Secretaria d'Universitats i Recerca del Departament d'Empresa i Coneixement de la Generalitat de Catalunya).

REFERENCES

Masato Aoki et al. 2007. Dependence of band structures on stacking and field in layered graphene. *Solid State Communications* 142, 3 (2007), 123–127.

Florian Banhart et al. 2011. Structural Defects in Graphene. *ACS Nano* 5, 1 (2011), 26–41. https://doi.org/10.1021/nn102598m

Cristina Bena et al. 2009. Remarks on the tight-binding model of graphene. *New Journal of Physics* 11, 9 (2009), 095003.

Leonor Chico et al. 1996. Quantum conductance of carbon nanotubes with defects. *Phys. Rev. B* 54 (Jul 1996), 2600–2606. Issue 4. https://doi.org/10.1103/PhysRevB.54.2600

Hao-Ting Chin et al. 2018. Impact of growth rate on graphene lattice-defect formation within a single crystalline domain. *Scientific Reports* 8 (12 2018). https://doi.org/10.1038/s41598-018-22512-5

Sorin Cotofana et al. 2018. On graphene nanoribbon-based nanoelectronic circuits viability. In *Proc. 42nd Workshop Compound Semicond. Devices Integr. Circuits Held Eur.* 35–36.

Supriyo Datta. 2000. Nanoscale device modeling: the Green's function method. *Superlattices and microstructures* 28, 4 (2000), 253–278.

Supriyo Datta. 2005. *Quantum transport: atom to transistor.* Cambridge university press.

Supriyo Datta. 2012. *Lessons from nanoelectronics: a new perspective on transport.* Vol. 1. World Scientific publishing company.

Houk Jang et al. 2016. Graphene-based flexible and stretchable electronics. *Advanced Materials* 28, 22 (2016), 4184–4202.

Yande Jiang et al. 2018. On carving basic Boolean functions on graphene nanoribbons conduction maps. In *2018 IEEE International Symposium on Circuits and Systems (ISCAS)*. IEEE, 1–5.

Yande Jiang et al. 2019. Graphene nanoribbon based complementary logic gates and circuits. *IEEE Transactions on Nanotechnology* 18 (2019), 287–298.

Ioannis G. Karafyllidis. 2014. Current Switching in Graphene Quantum Point Contacts. *IEEE Transactions on Nanotechnology* 13, 4 (2014), 820–824.

Xinming Li et al. 2017. Graphene and related two-dimensional materials: Structure-property relationships for electronics and optoelectronics. *Applied Physics Reviews* 4, 2 (2017), 021306.

Lili Liu et al. 2015. Defects in Graphene: Generation, Healing, and Their Effects on the Properties of Graphene: A Review. *Journal of Materials Science & Technology* 31, 6 (2015), 599 – 606. https://doi.org/10.1016/j.jmst.2014.11.019 A Special Issue on 1D Nanomaterials.

Savvas Moysidis et al. 2018. Graphene Logic Gates. *IEEE Transactions on Nanotechnology* 17, 4 (2018), 852–859.

Savvas Moysidis et al. 2020. Conductance Parametric Analysis of Graphene Nanoribbons With Magnetic Contacts. *IEEE Transactions on Nanotechnology* 19 (2020), 778–783.

Konstantin S. Novoselov et al. 2004. Electric Field Effect in Atomically Thin Carbon Films. *Science* 306, 5696 (2004), 666–669. https://doi.org/10.1126/science.1102896

Konstantin S. Novoselov et al. 2007. Room-Temperature Quantum Hall Effect in Graphene. *Science* 315, 5817 (2007), 1379–1379. https://doi.org/10.1126/science.1137201

Konstantinos Rallis et al. 2021. Electronic properties of graphene nanoribbons with defects. *IEEE Transactions on Nanotechnology* 20 (2021), 151–160.

Konstantinos Rallis et al. 2018. Multi-valued logic circuits on graphene quantum point contact devices. In *Proceedings of the 14th IEEE/ACM International Symposium on Nanoscale Architectures*. 44–48.

Stephanie Reich et al. 2002. Tight-binding description of graphene. *Physical Review B* 66, 3 (2002), 035412.

Wenchao Tian et al. 2017. A Review on Lattice Defects in Graphene: Types, Generation, Effects and Regulation. *Micromachines* 8, 5 (May 2017), 163. https://doi.org/10.3390/mi8050163

He Wang et al. 2020. Ultra-compact, entirely graphene-based nonlinear leaky integrate-and-fire spiking neuron. In *2020 IEEE International Symposium on Circuits and Systems (ISCAS)*. IEEE, 1–5.

Matthew Yankowitz et al. 2019. Tuning superconductivity in twisted bilayer graphene. *Science* 363, 6431 (2019), 1059–1064.

Yanhui Zhang et al. 2016. Invisible growth of microstructural defects in graphene chemical vapor deposition on copper foil. *Carbon* 96 (2016), 237–242.